Synthesis and characterization of power efficient triboelectric nanogenerator based on contact-separation mode using spray pyrolysis

Ashish Singh Sambyal[1], Deepak Anand[1], Rakesh Vaid[1,*], and Nandu B Chaure[2,*]

[1] *Department of Electronics, University of Jammu, Jammu, J&K 180006, India*
[2] *Department of Physics, Savitribai Phule Pune University, pune 411007, India*

ABSTRACT

Herein, a novel triboelectric nanogenerator (TENG) based on fluorine tin oxide (FTO) as substrate, metallic copper (Cu), and Polydimethyl siloxane (PDMS) as transparent and flexible polymer materials with spray pyrolysis of gold nanoparticles (AuNPs) has been synthesized and characterized having dimensions of 1.5×1.5 cm. The spherical shaped synthesized AuNPs have been observed within the morphological images. The x-ray diffraction pattern of the prepared material shows an accurate diffraction peaks at 2theta values indicating the presence of mixed phases of FTO, Cu, AuNPs, and PDMS which are in excellent agreement with the previously mentioned 2theta values in the literature. Further, the energy dispersive spectroscopy (EDS) analysis confirms the presence of Cu, gold (Au), oxygen (O), tin (Sn), carbon (C) and silicon (Si) materials within the synthesized TENG. Finally, the synthesized PDMS-based TENG produces maximum AC output voltage and current up to ~ 56 V and ~ 18 mA, respectively with very high transmittance of 92.85% along with a transferred electric charge of ~ 18 nC, current density of ~ 8 mA/cm^2, an output power of ~ 1 W, and a surface power density of ~ 448 mW/cm^2 with resistance of 3 KΩ. The TENG device is further connected with a bridge-type rectifier circuit to glow LEDs as well as serve as a platform for flexible and wearable electronic devices.

1 Introduction

Due to simple fabrication, scalability, and more energy conversion efficiency, different types of triboelectric nanogenerators (TENG) have attracted much attention [1, 2]. Wang along with their co-workers coupled a variety of TENGs based on triboelectric effect and electrostatic induction and convert mechanical energy into electrical energy with the ability to harvest an enormous amount of waste

energy from everyday human activities [3–9]. There are four basic modes in TENG: Contact-separation, single-electrode, contact-sliding, and free-standing mode. To increase charge density between two different materials, some metals, polymers, and crystalline materials are selected from triboelectric series which are arranged in sequences of their ability to lose or gain electrons [10–13]. Fluorine-doped tin oxide (FTO) is an n-type wide band gap transparent conducting oxide (TCO) has been invariably used in optoelectronic devices, including solar cells while FTO substrates were frequently utilized as transparent electrodes [14] due to its cost-effectiveness and strong chemical and thermal stability [15]. Notably, the increased electrical conductivity of the metal layer makes its inclusion capable of improving the conductivity of the FTO single-layer film [16]. On the other hand, PDMS became a most popular and suitable triboelectric material owing to its strong electro negativity, transparency and flexibility for output performance of TENG devices [17–19] and occupies a particular position in the triboelectric series. The authors Zhao et al., [20], demonstrated a rain drop energy harvesting by using two-electrode Ag/PDMS hybrid tandem solar cell based TENG to increase power conversion efficiency and while Y. Liu et al. [21] used mutual electrode having imprinted-PDMS with integrating silicon based solar cell as one of the triboelectric layers. AuNPs are used because they can enhance surface charge density and have more qualities like high surface-to-volume ratio, strong conductivity, extremely high surface energy and excellent molecule recognition [22]. The generation of electrons from the top layer to the electrode surface has been greatly aided by AuNPs because of their distinct physical and chemical characteristics. Many researches have illustrated surface engineering on the surface of metals, such as the deposition of AuNPs in various sizes and forms. Gold has been employed in many applications because, unlike other metals, it is highly resistant to the oxygen present in the air and can therefore be used without fear of oxidation or corrosion. Furthermore, without using a complicated fabrication technique, it is simple to synthesize AuNPs in a variety of shapes and sizes, resulting in a high contact surface area at ambient temperature and pressure for improvement to the metal's surface. In comparison to the metal without any surface engineering, the output characteristics of the metal improved with the deposition of AuNPs on its surface. Due to gold's resistance to oxygen, utilizing AuNPs has the additional benefit of not requiring specific packaging to safeguard the TENG device [23, 24]. The proposed TENG is operated in vertical contact-separation mode with two different materials chosen from the triboelectric series having opposite electric charges are separated by a sponge as a spacer. In this paper, we developed a low cost, simple TENG mainly consisting of Metal-Polymer materials: Cu, AuNPs and PDMS. Cu with AuNPs metal layer was chosen as the positive material which lose electrons and PDMS as a negative layer which gain electrons during triboelectrification. Due to tribo charging, as the materials are separated, they create friction. This frictional force deposits excess of electrons from one material and draws electrons away from other material, leaving a negative or positive electrical charge on both materials. On pressing these materials by external mechanical force, electrostatic charges are developed across them, while on release; an induced charge develops a potential drop which generates an alternating voltage between them. Figure 1 demonstrates the working mechanism of Cu-PDMS-based TENG showing a contact-separation cycle [Fig. 1a–d] consists of layers of FTO/Cu/AuNPs and FTO/PDMS. On pressing and releasing the spacer [sponge] is used for regaining the original position of TENG at different time intervals. Figure 2a shows the schematic diagram of TENG and whereas the Fig. 2b, c shows the steps of deposition of the upper part of TENG. In step 1, Cu was deposited on FTO by magnetron sputtering and in step 2, freshly prepared AuNPs are deposited on Cu using spray pyrolysis for increasing the surface roughness of layer1. In step3, in the lower part of TENG; PDMS is deposited on FTO by spin coating. An output AC pulse voltage has been achieved which is further connected to the power management system to convert it into DC voltage to glow light-emitting diodes or for any other relevant applications.

2 Experimental details

The synthesized TENG consists of two parts; the upper and lower part. The sponge is placed as a spacer layer between the lower part and the upper part. The synthesized upper part of TENG consists of three layers such as FTO/Cu/AuNPs whereas the lower part of the synthesized TENG consists of two

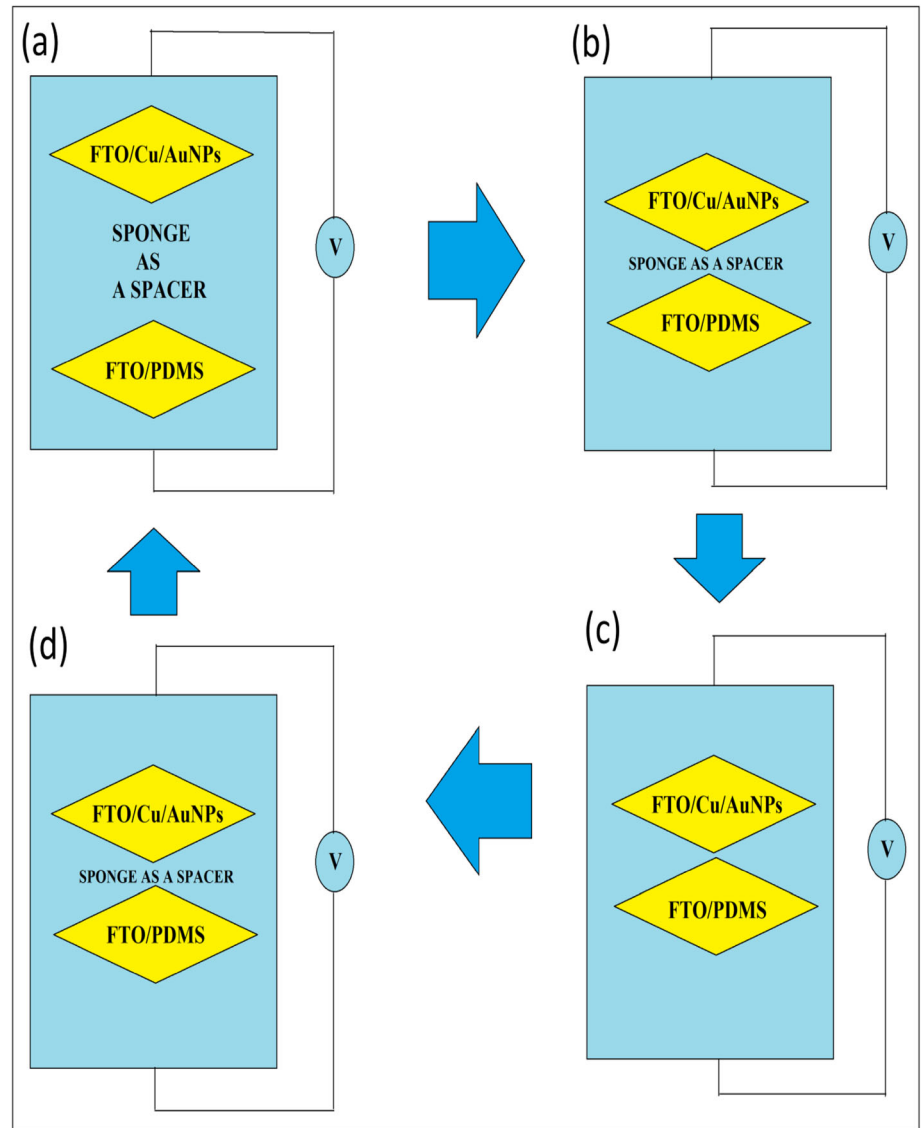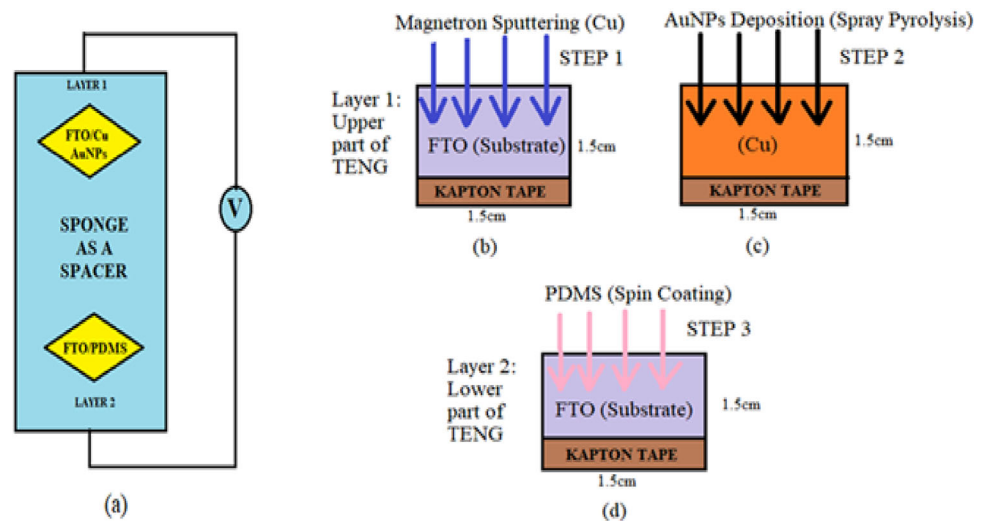**Fig. 1** Working mechanism of Cu-PDMS based TENG

Fig. 2 a–d Schematic diagram and steps of deposition of Cu-PDMS-based TENG

layers such as FTO/PDMS. The dimensions of the FTO substrate are of the order of 1.5 × 1.5 cm. The substrate was cleaned with soap solution, and then sonicated for 15 min, and stored in Isopropyl alcohol (IPA) solution. Subsequently, the Cu target surface was polished and cleaned with ethanol solution. The FTO substrate was covered with Kapton before the sputtering process followed by placing all the samples in the sputtering chamber facing conducting sides upward opposite to the Cu target at a working pressure of $5.8 × 10^2$ mbar, power of 160 W, flow of 80 sccm for 10 min at a temperature of 200 °C. Next, the AuNPs having spherical shapes are deposited on Cu using spray pyrolysis. In this way, the upper part of the TENG was synthesized. Now by taking an FTO substrate, the PDMS emulsion of 5 ml was added in 20 ml of chloroform and magnetically stirred at 500 rpm for 10 min without heating. Then spin coating technique was used for the deposition of PDMS on FTO at 2000 rpm for 30 s. Then, the sample was annealed in a muffle furnace at 300 °C for 6 h to approach a thickness in the micrometer range. In this way, the lower part of TENG was synthesized. Finally, by using a sponge as a spacer, the lower and upper part of TENG has been covered by transparent tape. The Kapton tape was removed after deposition from both the layers so that on pressing and releasing, the triboelectric charge and electrostatic induction are developed across the two parts which further generates the potential difference in form of AC voltage and current.

3 Results and discussion

Scanning electron microscope (SEM) images were recorded using Model JEOL JSM 6360 A with an energy ranging from 0.5 to 40 KeV. The material's presence in the sample was observed by energy dispersive spectroscopy (EDS). X-ray diffraction (XRD) measurements were performed by using D8 ADVANCE (BRUKER AXS) equipment with the source of light Cu Kα (λ = 1.5406A°) radiation. The optical characterization was performed by using a UV-Vis spectrophotometer (JASCO V-770) in the 200–1000 nm spectral region. The electrical characterization measures open-circuit voltage and short-circuit current using DSOX6004A. Micro-structured characterization of Raman shift was measured by

using Raman spectroscope with a laser as the light source excitation wavelength of 785 nm.

3.1 Materials characterization

The working mechanism of Cu-PDMS based TENG has been illustrated on Fig. 1. The FTO serves as a non-flexible substrate for the vertical contact-electrification process. Figure 3a–d shows the morphological images of FTO/Cu/AuNPs for thicknesses of 5, 2, 1, and 0.5 μm wherein it is clearly observed that the AuNPs possess a typical spherical shape which increases the surface density to generate more triboelectric charges between the two contact surfaces in TENG device. Figure 3e–h shows the morphological images of FTO/PDMS for thicknesses of 5, 2, 1 and 0.5 μm. The XRD pattern of the FTO substrate is demonstrated in Fig. 4a which is assigned to tetragonal Tin Oxide (SnO_2) (JCPDS file: 77–0452). The peaks in the XRD pattern correspond to the standard values of face-centered cubic (FCC) structure at (110), (101), (200), (220), (221), and (301). The highest peak is obtained at an angle of 26° with an intensity of 440 a.u. At an angle of 43.44° (111), the maximum peak of diffraction is at 210 a. u. in Fig. 4b. The other peak is at 51.56° (220) confirming metallic copper which is in agreement with the previously published result in the literature [25]. In Fig. 4c, the XRD pattern reveals that the top diffraction peak is at 38.26° and another diffraction peak is at 66.29° which corresponds to the reflection of the FCC structure of gold having a good agreement with the previously reported studies [26].

Figure 4d show the spray pyrolysis results of AuNPs on FTO/Cu and the combined peaks of FTO, Cu, and Au which enhance the crystal structure and purity of the upper layer of TENG. The AuNPs shows crystalline high sharp peak at 180a.u having FCC structure. FTO shows the highest peak intensity at 230a.u. The broad diffraction peak intensity is continuously decreasing from 20° to 70°. To further confirm the presence of Cu, Sn, O, Si, and Au within the synthesized lower part (FTO/PDMS) and upper part (FTO/Cu/AuNPs) of the TENG, the samples were analyzed by energy dispersive X-ray spectroscopy (EDS) technique as shown in Fig. 5a and b. The EDS analysis reveals that a high optical absorption band peak at 1 KeV, and a low optical absorption peak at 8.9 KeV confirm the presence of metallic copper in the sample [25, 26]; an optical absorption band peak at approximately 1.9, 2.2 and 8.5 KeV
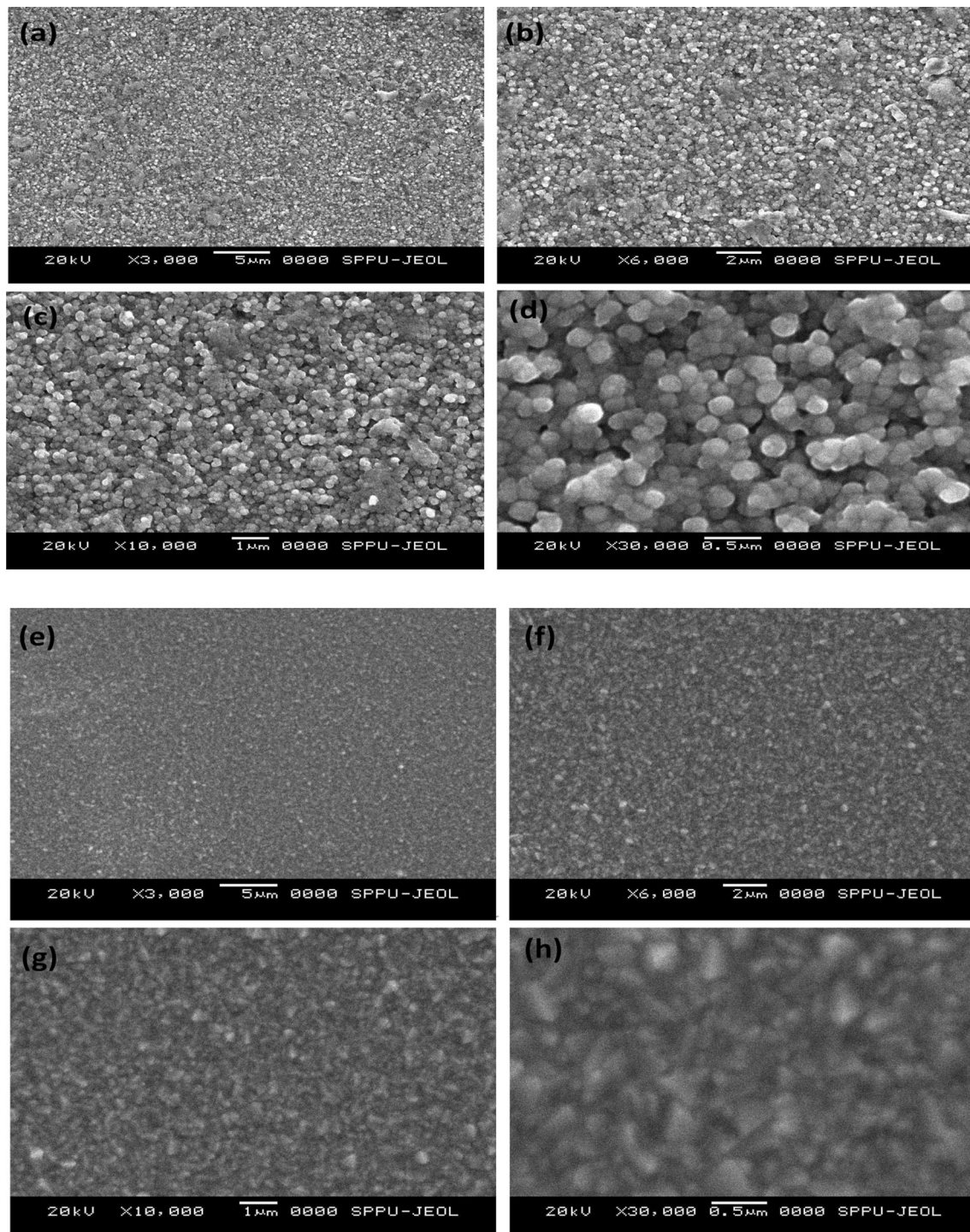
Fig. 3 **a–d** Morphological images of FTO/Cu/AuNPs and **e–h** Morphological images of FTO/PDMS

confirms the presence of gold in the sample similar to as observed in the previous experimental study[27] where a maximum optical absorption band peak at approximately 3.5 KeV confirms the presence of Sn in the PDMS sample [25]. A similar optical absorption band peak at approximately 0.5 KeV confirms the presence of oxygen in both the samples [25, 27]. An optical absorption band peak at 1.9 KeV confirms the presence of Si in the sample and an optical absorption band peak at 0.2 KeV confirms the presence of C on
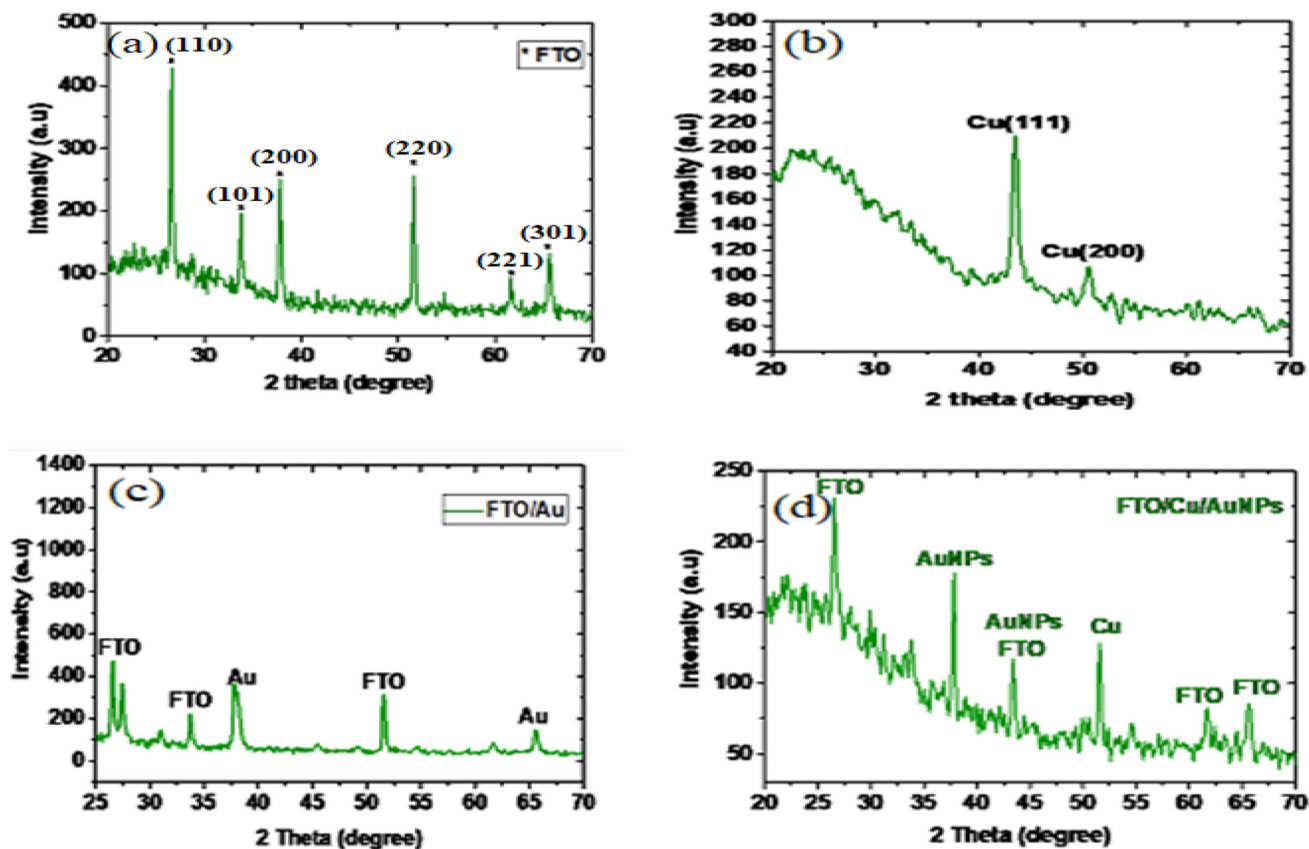
Fig. 4 a–d XRD of upper part of TENG: **a** FTO substrate, **b** FTO/Cu, **c** FTO/AuNPs and **d** FTO/Cu/AuNPs
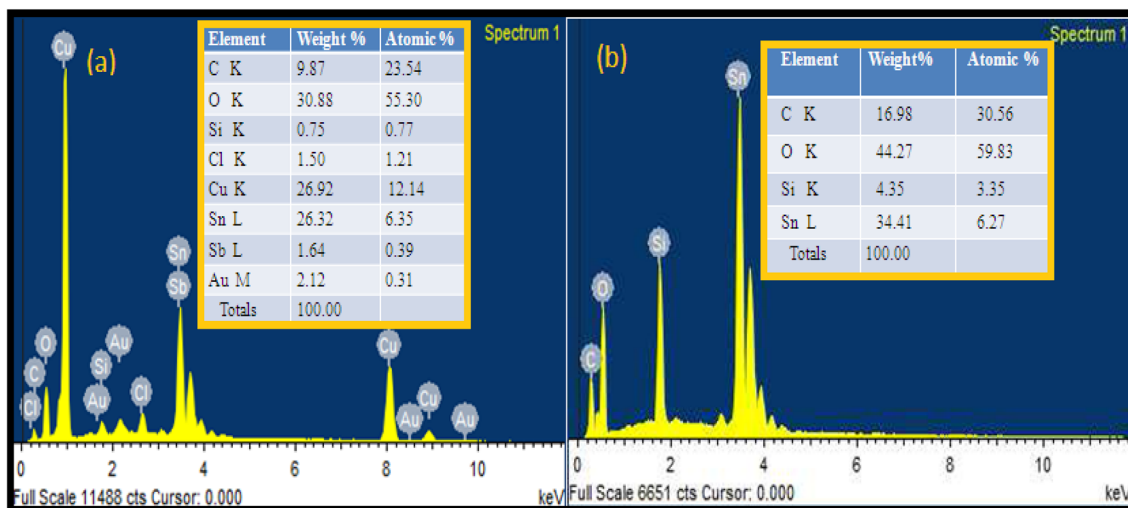

Fig. 5 **a** and **b** EDS patterns of upper part consisting of FTO/Cu/AuNPs and lower part FTO/PDMS

the sample. The EDS spectra of the FTO/Cu/AuNPs and FTO/PD MS samples are shown in Fig. 5 a, b to evaluate the contents of elements on the upper part and lower part of the TENG. The FTO/Cu/AuNPs were composed of O (30.88%), Cu (26.33%), Sn (26.33), C (9.87%), and a trace amount of Au (2.12%), Si (0.75%), Cl (1.50%). The FTO/PDMS was mainly composed of O (44.27%), Sn (34.41%), C (16.98%) and trace amount of Si (4.35%).
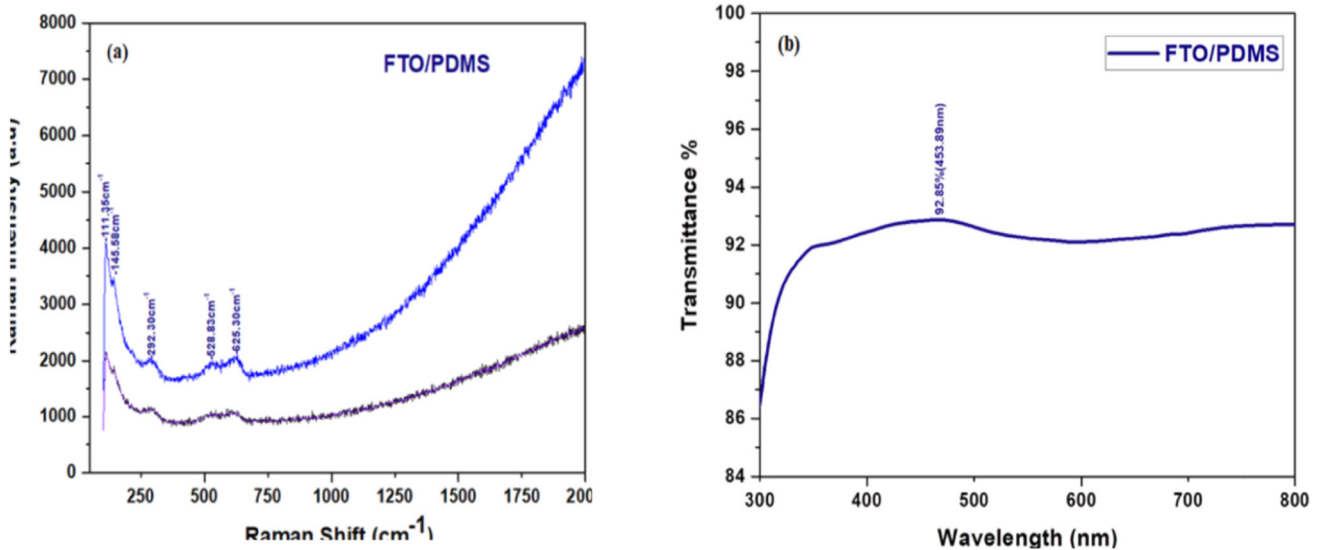
Fig. 6 **a** and **b** Open-circuit voltage (V_{OC}) during pressing and releasing and **c** and **d** short-circuit current (I_{SC}) during pressing and releasing of a Cu-PDMS based TENG

3.2 Optical characterization

To identify the nature of the charged molecules, using Raman spectroscopy we performed a comparative experiment at different laser intensities. Figure 6a shows the comparison of Raman shift (cm^{-1}) at 8000 and 3000 a.u. Raman shifts at 528.83 and 625.30 cm^{-1} of a lower graph show a wide curve whereas the upper graph at the same shift shows a narrower peak at higher intensities. As the Raman intensity increases from 1000 to 4000 a.u, Raman shift peaks become a little sharper than the lower graph curve. Transmittance (T) indicates the ratio of the intensity of light after passes through sample (I) to the initial intensity of light (I_O) and it can be calculated as $T = I/I_O$. The % $T = I/I_O \times 100$. Figure 6b represents the transmittance of transparent PDMS polymer material measured by the UV-Visible spectroscopy technique. The transmittance is plotted within the wavelength range of 300–800 nm. It is clearly seen that the light easily passes through the prepared PDMS polymer material used for the synthesis of TENG with a maximum transmittance of $\sim$ 92.85% at the wavelength of 453.89 nm which provides us with another effective way for the development of transparent electronic devices.

3.3 Electrical output performance characterization

The upper part of TENG consists of FTO/Cu/AuNPs which is highly triboelectrically positive, whereas the lower part of TENG consists of FTO/PDMS surface which is negatively charged. The two parts are separated by spacer layer (sponge) which supports both the parts to come back to the original position after pressing and releasing of the TENG. On pressing by external mechanical force, electrostatic charges are developed across them and on releasing, an induced charge develops a potential drop which generates an alternating voltage between them. Figure 7a shows the pictured view of AC output voltage generated and Fig. 7b shows the synthesized PDMS-based TENG. Figure 8a and b shows open-circuit voltage during pressing and releasing and Fig. 8c and d shows the short-circuit current during pressing and releasing of a PDMS-based TENG. By applying external mechanical force, the process of pressing the TENG with the finger will produce an AC sine wave with an maximum open-circuit voltage (V_{OC}) of $\sim$ 56 V, an short-circuit current (I_{SC}) of $\sim$ 18 mA, transferred electric charge of $\sim$ 18 nC, output power of $\sim$ 1 W, current density of $\sim$ 8 mA/cm^2, and surface power density of $\sim$ 448 mW/cm^2. On releasing, it generates an open-circuit voltage of $\sim$ 14 V, an short-circuit current of $\sim$ 15mA, transferred electric charge of $\sim$ 15 nC, output power of $\sim$ 210 mW, current

Fig. 7 a Pictured view of AC output voltage **b** Synthesized Cu-PDMS based TENG
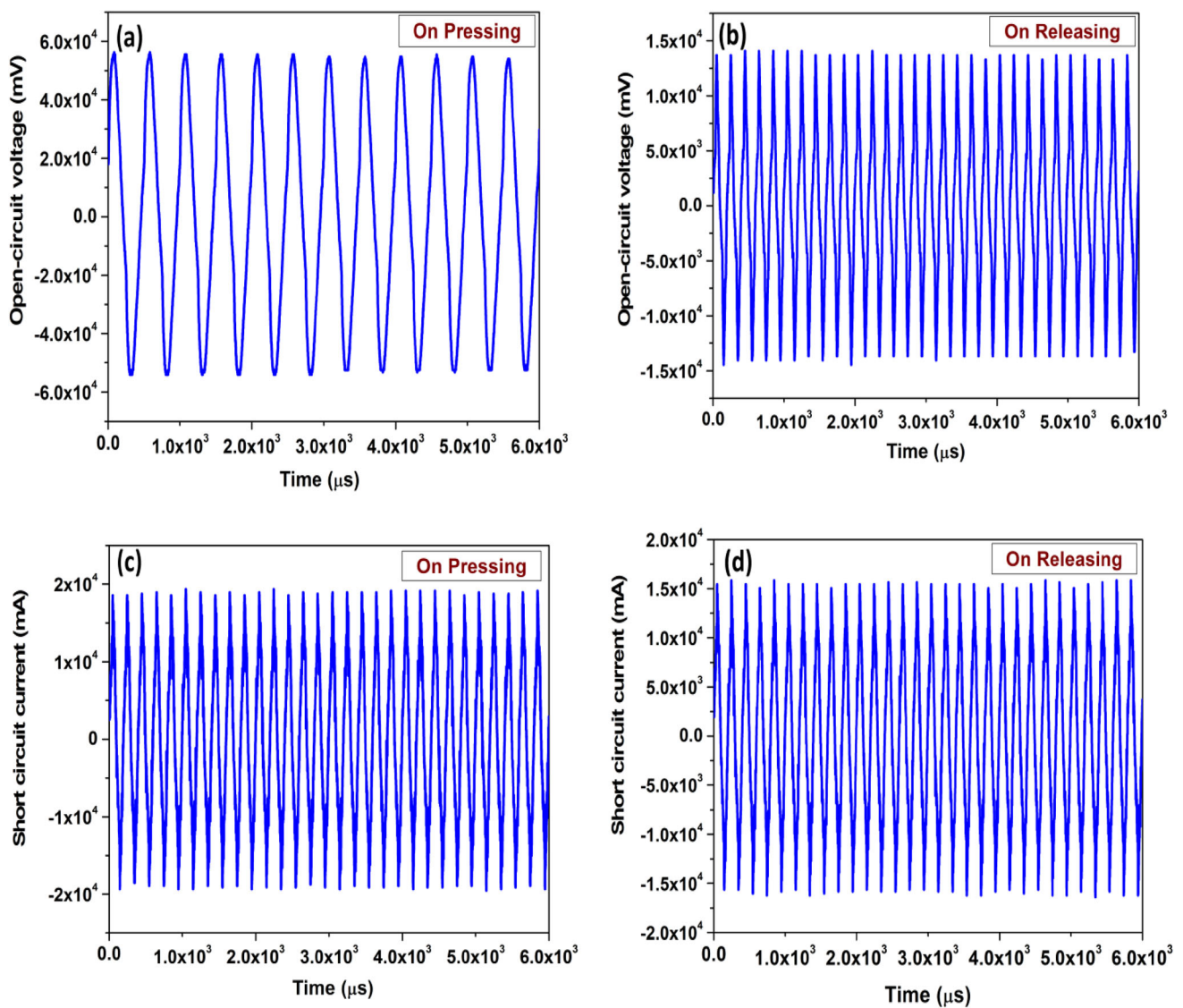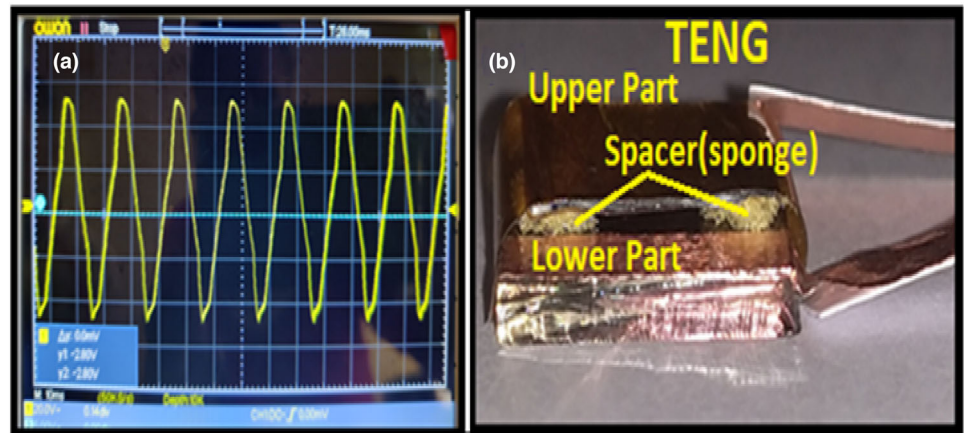

Fig. 8 a and **b** Open-circuit voltage (V_{OC}) during pressing and releasing and **c** and **d** short-circuit current (I_{SC}) during pressing and releasing of a Cu-PDMS based TENG

density of $\sim 6.7\,\mathrm{mA/cm^2}$, and surface power density of $\sim 93\,\mathrm{mW/cm^2}$ with an resistance between 1KΩ–3KΩ.

4 Conclusions

In the current research work, a transparent and flexible PDMS-based TENG with spray pyrolysis of AuNPs has been synthesized and characterized successfully. The spherical shapes of the synthesized AuNPs have been observed within the morphological images. The XRD pattern of the prepared sample indicates the diffraction peaks of FTO, Cu, and AuNPs at different 2theta values. The EDS analysis further confirms the presence of O, Cu, Sn, C, Au, Cl, and Si materials within the synthesized parts of TENG while the UV-Visible spectroscopy analysis clearly shows 92.85% light transmission and further, the proposed synthesized PDMS-based TENG generate energy in the form of AC output voltage up to ~ 56 V and current signal of ~ 18 mA, respectively. Finally, it has been concluded that the synthesized PDMS-based TENG with Spray pyrolysis of AuNPs is useful for optical devices in the generation of light. The electrical energy in terms of AC voltage produced by synthesized PDMS-based TENG is further converted into DC voltage by using a power management system that provides a platform for wearable electronic devices, mobile chargers, LEDs, and power supplies to different electronic circuits in the future.

Author contributions

ASS—Material preparation, data collection, formal analysis, and the writing of the first draft of the manuscript. DA—contributed to the experimentation, data collection, and formal analysis. RV—Conceptualization, Writing—Review and Editing, Project administration, Funding acquisition, Supervision. NBC—Conceptualization, Writing—Review and Editing.

Data availability

The data produced during the experiments are available within the manuscript.

Declarations

Competing interests The authors declare that there exists no conflict of financial or non-financial interests related to the work submitted for publication.

References

1. T.C. Hou, Y. Yang, H. Zhang, J. Chen, L.J. Chen, Z.L. Wang, Triboelectric nanogenerator built inside shoe insole for harvesting walking energy. Nano Energy. **2**(5), 856–862 (2013). https://doi.org/10.1016/j.nanoen.2013.03.001
2. G. Zhu, J. Chen, Y. Liu, P. Bai, Y.S. Zhou, Q. Jing, C. Pan, Z.L. Wang, Linear-grating triboelectric generator based on sliding electrification. Nano Lett. **13**(5), 2282–2289 (2013). https://doi.org/10.1021/nl4008985
3. F. Mugele, Baret electrowetting: from basics to applications. J. Phys. **17**(28), R705–R774 (2005). https://doi.org/10.1088/0953-8984/17/28/r01
4. Y. Chen, J. Au, P. Kazlas, A. Ritenour, H. Gates, M. McCreary, Flexible active-matrix electronic ink display. Nature. **423**(6936), 136–136 (2003). https://doi.org/10.1038/423136a
5. S. Kim, H.J. Kwon, S. Lee, H. Shim, Y. Chun, W. Choi, J. Kwack, D. Han, M. Song, S. Kim, S. Mohammadi, I. Kee, Low-power flexible organic light-emitting diode display device. Adv. Mater. **23**(11), 3511–3516 (2011). https://doi.org/10.1002/adma.201101066
6. B. Yoon, D.Y. Ham, O. Yarimaga, H. An, C.W. Lee, J.M. Kim, Inkjet printing of conjugated polymer precursors on paper substrates for colorimetric sensing and flexible electrothermochromic display. Adv. Mater. **23**(46), 5492–5497 (2011). https://doi.org/10.1002/adma.201103471
7. H.H. Chou, A. Nguyen, A. Chortos, J.W.F. To, C. Lu, J. Mei, T. Kurosawa, W.G. Bae, J.B.H. Tok, Z. Bao, A chameleon-

inspired stretchable electronic skin with interactive colour changing controlled by tactile sensing. Nat. Commun. **6**(1), 8011 (2015). https://doi.org/10.1038/ncomms9011

8. T. Zhou, C. Zhang, C.B. Han, F.R. Fan, W. Tang, Z.L. Wang, Woven structured triboelectric nanogenerator for wearable devices. ACS Appl. Mater. Interface. **6**(16), 14695–14701 (2014). https://doi.org/10.1021/am504110u

9. Y. Yang, H. Zhang, Z.H. Lin, Y.S. Zhou, Q. Jing, Y. Su, J. Yang, J. Chen, C.C. Hu, Z.L. Wang, Human skin based triboelectric nanogenerators for harvesting biomechanical energy and as self-powered active tactile sensor system. ACS Nano **7**(10), 9213–9222 (2013). https://doi.org/10.1021/nn403838y

10. Z.L. Wang, *Springer International Publishing*: Cham, Switzerland, 2016, pp.1–99

11. S. Pan, Z. Zang, Fundamental theories and basic principles of triboelectric effect. Rev. Frict. **7**, 2–17 (2018). https://doi.org/10.1007/s40544-018-0217-7

12. L.S. McCarty, G.M. Whitesides, Electrostatic charging due to separation of ions at interfaces: contact electrification of ionic electrets Angew. Chem. Int. Ed. **47**(12), 2188–2207 (2008). https://doi.org/10.1002/anie.200701812

13. K. Friedrich, Polymer composites for tribological applications. Adv. Ind. Eng. Polym. Res. **1**, 3–39 (2018). https://doi.org/10.1016/j.aiepr.2018.05.001

14. S.J. Peng, F.Y. Cheng, J. Liang, Z.L. Tao, J. Chen, Facile solution-controlled growth of CuInS2 thin films on FTO and TiO$_2$/FTO glass substrates for photovoltaic application. J. Alloys Compd. Alloys Comp. **481**(1–2), 786–791 (2009). https://doi.org/10.1016/j.jallcom.2009.03.084

15. B.G. Lewis, D.C. Paine, M.R.S. Bull, Applications and processing of transparent conducting oxides. MRS Bull. **25**(08), 22–27 (2000). https://doi.org/10.1557/mrs2000.147

16. N.F. Ren, L.J. Huang, M. Zhou, B.J. Li, Introduction of Ag nanoparticles and AZO layer to prepare AZO/Ag/FTO trilayer films with high overall photoelectric properties. Ceram. Int. **40**(6), 8693–8699 (2014). https://doi.org/10.1016/j.ceramint.2014.01.087

17. F.R. Fan, J.J. Luo, W. Tang, C.Y. Li, C.P. Zhang, Z.Q. Tian, Z.L. Wang, Highly transparent and flexible triboelectric-nanogenerator: performance improvements and fundamental mechanisms. J. Mater. Chem. A **2**, 13219–13225 (2014). https://doi.org/10.1021/nn507221f

18. W. Seung, M.K. Gupta, K.Y. Lee, K.S. Shin, J.H. Lee, T.Y. Kim, S. Kim, J.J. Lin, J.H. Kim, S.W. Kim, Nano patterned textile-based wearable triboelectric nanogenerator. ACS Nano. **9**, 3501–3509 (2015). https://doi.org/10.1021/nn507221f

19. S.H. Lee, Y.H. Ko, J.S. Yu, Facile fabrication and characterization of arch-shaped triboelectric nanogenerator with a graphite top electrode. Phys. Status Solidi. A **212**, 401–405 (2014). https://doi.org/10.1002/pssa.201431480

20. L. Zhao, J. Duan, L. Liu, J. Wang, Y. Duan, L. Vaillant-Roca, X. Yang, Q. Tang, Boosting power conversion efficiency by hybrid triboelectric nanogenerator/silicon tandem solar cell toward rain energy harvesting. Nano Energy. **82**, 105773 (2021). https://doi.org/10.1016/j.nanoen.2021.105773

21. Y. Liu, N. Sun, J. Liu, Z. Wen, X. Sun, S.-T. Lee, B. Sun, Integrating a silicon solar cell with a triboelectric nanogenerator via a mutual electrode for harvesting energy from sunlight and raindrops. ACS Nano **12**(3), 2893–2899 (2018). https://doi.org/10.1021/acsnano.8b00416

22. G. Presnova, D. Presnov, V. Krupenin, Biosensors based on a silicon nanowire field–effect transistor functionalized by gold nanoparticles for the highly sensitive determination of prostate specified antigen. Biosens. Bioelectron. **88**, 283–289 (2017). https://doi.org/10.1016/j.bios.2016.08.054

23. H. Xiaopei, Y. Zhang, T. Ding, J. Liu, H. Zhao, Multifunctional gold nanoparticles: a novel nanomaterial for various medical applications and biological activities Front. Bioeng. Biotechnol. (2020). https://doi.org/10.3389/fbioe.2020.00990

24. G. Alberti, C. Zanoni, L.R. Magnaghi, R. Biesuz, Gold and silver nanoparticles-based calorimetric sensors new trends and applications. Chemosensors. **9**(11), 305 (2021). https://doi.org/10.3390/chemosensors9110305

25. A. Sahai, N. Goswami, S.D. Kaushik, S. Tripathi, Cu$_2$O/CuO nanoparticles: novel synthesis by exploding wire technique and extensive characterization. Appl. Surf. Sci. **390**, 974–983 (2016). https://doi.org/10.1016/j.apsusc.2016.09.005

26. A. Aravinthan, S.K. Kannan, M. Govarthanan, J.H. Kim, Accumulation of biosynthesized gold nanoparticles and its impact on various organs of sprague dawley rats: a systematic study. Toxicol. Res. **5**(6), 1530–1538 (2016). https://doi.org/10.1039/c6tx00202a

27. J. Zhu, P. Zhu, Q. Yang, T. Chen, J. Wang, J. Li, A fully stretchable textile-based triboelectric nanogenerator for human motion monitoring. Mater. Lett. **280**, 128568 (2020). https://doi.org/10.1016/j.matlet.2020.128568